

SCREENING OF THE MAGNETIC FIELD OF DISK ACCRETING STARS

R. V. E. LOVELACE AND M. M. ROMANOVA

Department of Astronomy, Cornell University, Ithaca, NY 14853; rv11@cornell.edu, romanova@astro.cornell.edu

AND

G. S. BISNOVATYI-KOGAN

Space Research Institute, Russian Academy of Sciences, Moscow, Russia; gkogan@mx.iki.rssi.ru

Received 2004 November 10; accepted 2005 February 5

ABSTRACT

An analytical model is developed for the screening of the external magnetic field of a rotating, axisymmetric neutron star due to the accretion of plasma from a disk. The decrease of the field occurs as a result of the electric current in the infalling plasma. The deposition of this current-carrying plasma on the star's surface creates an induced magnetic moment with a sign opposite to that of the original magnetic dipole. The field decreases independent of whether the star spins up or spins down. The timescale for an appreciable decrease (factor of >100) of the field is found to be $\sim 1.6 \times 10^7$ yr, for a mass accretion rate $\dot{M} = 10^{-9} M_{\odot} \text{ yr}^{-1}$ and an initial magnetic moment $\mu_i = 10^{30} \text{ G cm}^3$, which corresponds to a surface field of 10^{12} G if the star's radius is 10^6 cm . The timescale varies approximately as $\mu_i^{3.8}/\dot{M}^{1.9}$. The decrease of the magnetic field does not have a simple relation to the accreted mass. Once the accretion stops the field leaks out on an Ohmic diffusion timescale that is estimated to be $>10^9$ yr.

Subject headings: pulsars: general — stars: magnetic fields — stars: neutron — X-rays: stars

1. INTRODUCTION

The decrease of the external magnetic field of accreting neutron stars has been a long-standing puzzle and has been explained as being due to Ohmic decay of the field (e.g., Goldreich & Reisenegger 1992), crustal motion on the star's surface (Ruderman 1991), or “burial” or screening of the original magnetic field by the accreted matter (Bisnovaty-Kogan & Komberg 1974). This work develops an analytic model for the decrease of the external field due to accretion of plasma.

For some time after the discovery of pulsars, only single-star objects were found. It appeared that pulsars did not occur in binaries. Because more than half of all stars are in binaries, the occurrence of isolated pulsars was explained either by pair disruption during supernova explosion leading to pulsar formation or by the absence of supernova explosions at the end of evolution of stars in close binaries (Trimble & Rees 1970). Bisnovaty-Kogan & Komberg (1974, hereafter BK74) analyzed the evolution of X-ray binaries in low-mass systems (e.g., Her X-1) and concluded that evolution of such systems should lead to the formation of nonaccreting neutron stars, i.e., radio pulsars, in close binary systems. BK74 showed that the neutron star rotation is accelerated during the disk accretion stage so that a reborn (or recycled) radio pulsar should become detectable provided its magnetic field is similar to that of isolated pulsars. The absence of radio pulsars in close binaries in extensive searches could be explained by only one reason (BK74): during the accretion stage the magnetic field of the neutron star is screened by the inflowing plasma, so that the recycled pulsar should have $B \sim 10^8\text{--}10^{10} \text{ G}$, which is 2–4 orders of magnitude smaller than the field strength of radio pulsars. Discovery of the first binary pulsar by Hulse & Taylor (1975), and subsequent discovery of more than 50 recycled pulsars (Bhattacharya & van den Heuvel 1991; Lorimer 2001; Lyne et al. 2004), confirmed the conclusion that recycled pulsars have small magnetic fields, as predicted by BK74.

From a statistical analysis of 24 binary radio pulsars with nearly circular orbits and low-mass companions, van den Heuvel

& Bitzaraki (1995) discovered a clear correlation between the spin period P and the orbital period P_{orb} , as well as between the magnetic field and the orbital period. The pulsar period and magnetic field strength increase with orbital period at $P_{\text{orb}} > 100$ days and scatter around $P \sim 3 \text{ ms}$ and $B \sim 2 \times 10^8 \text{ G}$ for smaller binary periods. These relations strongly suggest that an increase in the amount of accreted mass leads to a screening of the initial magnetic field and that there is a lowest field strength of about 10^8 G . Magnetic field screening during accretion has been discussed by a number of authors (see, e.g., BK74; Romani 1990; Wijers 1997; Cheng & Zhang 1998, 2000; Choudhuri & Konar 2002; Payne & Melatos 2004). The studies by Cheng & Zhang and by Payne & Melatos analyze the flow and magnetic field evolution *within* the neutron star, in contrast with the present work, which is concerned mainly with the magnetosphere of the star.

Here we present an analytical model of the screening of the magnetic field of a rotating neutron star due to the accretion of plasma from a disk. The system is assumed to be axisymmetric. In the idealized case of a nonconducting sphere, the decrease of the external magnetic field occurs because of the electric current in the infalling plasma. The accretion of this current-carrying plasma to the star's surface creates an induced magnetic moment with a sign opposite to that of the original magnetic dipole. In the more realistic case in which the star is treated as a conducting sphere, the magnetic field due to the accreted current-carrying plasma does not penetrate the main volume of the star. As a result the screening effect of the plasma is greatly reduced (compared with the case of a nonconducting star), and the timescale for appreciable screening is greatly increased. For representative parameters we find that the magnetic field of the conducting star decreases significantly on a timescale of the order of 10^7 yr. The screening mechanism stops working when the Alfvén radius is comparable to the radius of the star.

In § 2 the general picture is described, and the main equations are derived. In §§ 3 and 4 the magnetic field decrease during plasma accretion is considered for nonconducting and conducting

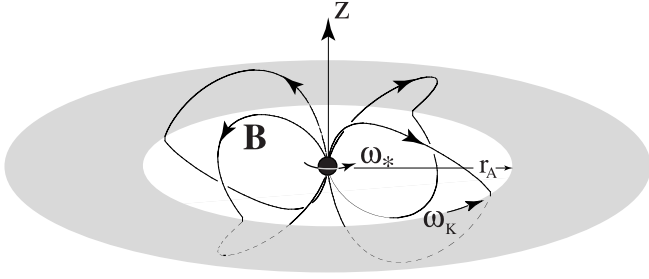


FIG. 1.—Three-dimensional view of four field lines going from the star to the Alfvén radius r_A . For the conditions shown the disk angular velocity at r_A , $\omega_K(r_A)$, is larger than the star's angular velocity ω_* .

spheres, respectively. We calculate the timescale for an appreciable decrease of the magnetic field of a conducting star, which depends on the radial thickness of the accreted matter. In § 5 we estimate the thickness of the accreted matter and the timescale for the magnetic field to diffuse out of the star once accretion has ceased. In § 6 we give the conclusions of this work.

2. THEORY

We consider disk accretion to a rotating neutron star with an aligned dipole magnetic field as indicated in Figure 1. That is, we consider an axisymmetric star, magnetic field, and disk. Further, we consider configurations that are mirror symmetric about the equatorial plane. We use both spherical (R, θ, ϕ) and cylindrical (r, ϕ, z) nonrotating coordinate systems.

For this system the corotation radius is

$$r_{\text{cr}} = \left(\frac{GM}{\omega_*^2} \right)^{1/3} \approx 1.7 \times 10^8 P^{2/3} \text{ cm}, \quad (1)$$

where ω_* is the angular rotation rate of the star, $P = 2\pi/\omega_*$ is its period, and the star's mass is considered to be $1.4 M_\odot$. The Alfvén radius r_A (or inner radius) of the disk is the distance at which the kinetic energy density of the matter $\rho v^2/2$ is comparable with the magnetic energy density $B^2/8\pi$ (Ghosh & Lamb 1979). This gives

$$r_A \approx k_A \left(\frac{\mu^2}{\dot{M} \sqrt{GM}} \right)^{2/7} \approx 1.94 \times 10^8 \left(\frac{k_A}{0.5} \right) \left(\frac{\mu_{30}^2}{\dot{M}_{-9}} \right)^{2/7} \text{ cm}. \quad (2)$$

Here μ or $\mu_{30} \equiv \mu/(10^{30} \text{ G cm}^3)$ is the star's magnetic moment, and \dot{M} or $\dot{M}_{-9} \equiv \dot{M}/(10^{-9} M_\odot \text{ yr}^{-1})$ is the mass accretion rate. The accretion luminosity is $L_{\text{accr}} = GMM/R_* \approx 1.2 \times 10^{37} \dot{M}_{-9}$ ergs s^{-1} assuming the star's radius $R_* = 10^6$ cm, while the Eddington luminosity for a $1.4 M_\odot$ star is $L_{\text{Edd}} \approx 1.76 \times 10^{38}$ ergs s^{-1} . Thus, $L_{\text{accr}}/L_{\text{Edd}} \approx 0.067 \dot{M}_{-9}$. The dimensionless coefficient k_A is of the order of one-half and depends weakly on the disk parameters (see Ghosh & Lamb 1979; Lovelace et al. 1995; Long et al. 2004). The star's accretion luminosity is $\dot{E}_a = GMM/R_* \approx 1.2 \times 10^{37} \dot{M}_{-9}$ ergs s^{-1} with the star's radius R_* assumed to be 10^6 cm.

The ratio r_A/r_{cr} determines the qualitative evolution of the system. For $r_A \lesssim r_{\text{cr}}$, accretion causes the star to spin up with the rate of increase of the angular momentum $dJ/dt \approx \dot{M}(GM r_A)^{1/2}$, where $J = I\omega_*$, with $I = 10^{45} I_{45} \text{ g cm}^2$ the star's moment of inertia. On the other hand, for $r_A \gtrsim r_{\text{cr}}$, the star spins down with the rate $dJ/dt \approx -\dot{M}(GM r_A)^{1/2}$. For $r_{\text{cr}} \ll r_A$ the star spins down but is in the propeller regime, in which an appreciable

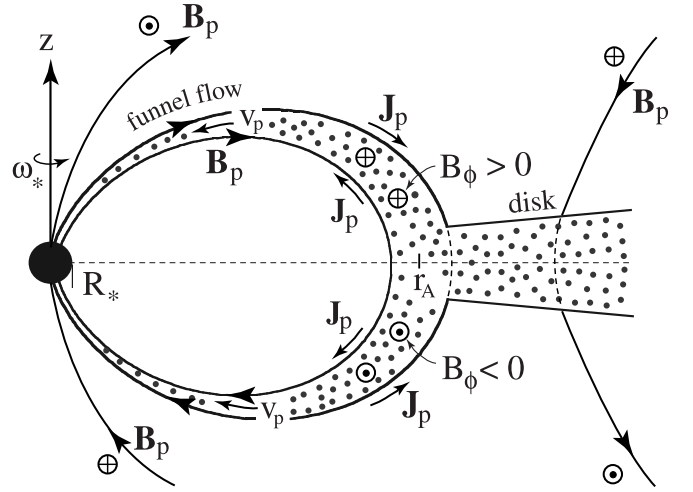


FIG. 2.—Diagram of the poloidal cross-section of the accretion disk and funnel flow. B_p is the poloidal magnetic field, B_ϕ is the toroidal magnetic field, J_p is the poloidal current density, and v_p is the poloidal component of the funnel flow velocity. The dotted circle represents an arrow out of the page, while the circle with the plus sign represents the opposite direction. The solid dots indicate a high plasma density.

fraction of the accreting matter may be expelled from the system by the rotating magnetosphere (Illarionov & Sunyaev 1975; Lovelace et al. 1999) or the accretion to the star's surface may be highly nonstationary (Romanova et al. 2004). In the propeller regime, the mass accretion rate in the outer disk (\dot{M} in eq. [2]) may be substantially larger than the mass accretion rate to the surface of the star (Lovelace et al. 1999). We consider only cases in which $r_A > R_*$, with R_* the star's radius.

For distances R less than r_A , the accreting matter moves in a “funnel flow,” which follows approximately the dipole magnetic field lines as sketched in Figure 2 (see, e.g., Romanova et al. 2002). For $R \ll r_A$ the velocity of the matter in the funnel flow is approximately free-fall. The cross-sectional area of the funnel flow S varies as R^3 for a dipole field so that $\rho \propto 1/R^{5/2}$. Consequently, $\rho v^2/2$ varies as $1/R^{7/2}$. Thus, the kinetic energy density of the funnel matter is much less than that of the magnetic field, which varies as $1/R^6$. Therefore, the funnel flow is magnetically dominated or force-free for $R < r_A$.

For the considered axisymmetric system, the magnetic field has the form

$$\mathbf{B} = \mathbf{B}_p + B_\phi \hat{\phi},$$

with $\mathbf{B}_p = B_R \hat{\mathbf{R}} + B_\theta \hat{\boldsymbol{\theta}}$. We can write

$$B_R = \frac{1}{R^2 \sin \theta} \frac{\partial \Psi}{\partial \theta}, \quad B_\theta = -\frac{1}{R \sin \theta} \frac{\partial \Psi}{\partial R},$$

where $\Psi(R, \theta) \equiv R \sin \theta A_\phi(R, \theta)$ is referred to as the “flux function.” Note that $\Psi(R, \theta) = \text{constant}$ is the equation for the poloidal projection of a magnetic field line.

In the force-free limit, the flow speeds are sub-Alfvénic, $v^2 \ll v_A^2 = B^2/4\pi\rho$, where v_A is the Alfvén velocity. In this limit, $\mathbf{J} \times \mathbf{B} \approx 0$; therefore, $\mathbf{J} = \lambda \mathbf{B}$ (Gold & Hoyle 1960). Because $\nabla \cdot \mathbf{J} = 0$, $(\mathbf{B} \cdot \nabla)\lambda = 0$ and consequently $\lambda = \lambda(\Psi)$. Thus, Ampère's equation becomes $\nabla \times \mathbf{B} = 4\pi\lambda(\Psi)\mathbf{B}/c$. The R - and θ -components of Ampère's equation imply that

$$H(\Psi) = R \sin \theta B_\phi \quad \text{and} \quad \frac{dH}{d\Psi} = \frac{4\pi}{c} \lambda(\Psi),$$

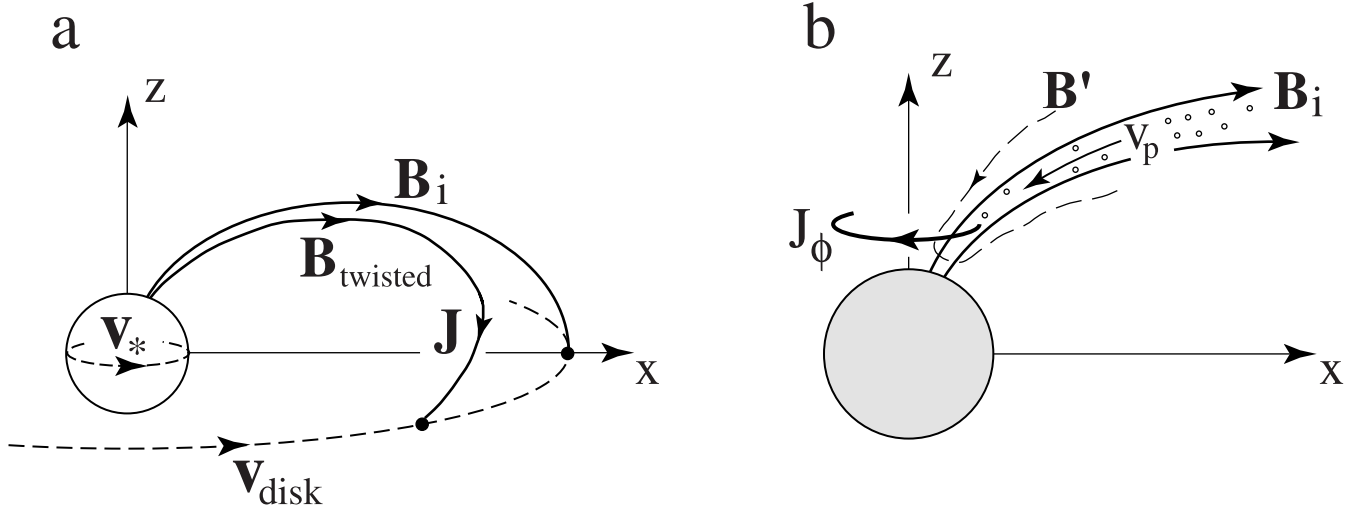


FIG. 3.—(a) Schematic drawing of an initial dipole field line \mathbf{B}_i (in the x - z plane) and the corresponding twisted field line for the case in which the angular velocity of the disk at the Alfvén radius $\omega_K(r_A)$ is *less* than the angular velocity of the star ω_* . This is opposite to the case shown in Figs. 1 and 2. The current flow \mathbf{J} parallel to the \mathbf{B} -field necessary to produce this twist is into the star at high latitudes and out of the star at low latitudes. The low-latitude current flow has the dominant screening effect, and only this current is shown in (a). This current flow along the twisted field line gives rise to a *negative* toroidal current density J_ϕ near the star as shown in (b). Panel (b) shows the poloidal field component \mathbf{B}' arising from the toroidal current J_ϕ . The funnel flow is indicated by the small circles, and the arrow \mathbf{v} indicates the flow velocity.

where $H(\Psi)$ is another function of Ψ . Thus, $H(\Psi) = \text{constant}$ along any given field line, and $\mathbf{J}_p = (c/4\pi)(dH/d\Psi)\mathbf{B}_p$ so that $(\mathbf{J}_p \cdot \nabla)H = 0$. The toroidal component of Ampère's equation gives

$$\Delta^* \Psi = -H(\Psi) \frac{dH(\Psi)}{d\Psi}, \quad (3)$$

where

$$\Delta^* \equiv \frac{\partial^2}{\partial R^2} + \frac{1 - \zeta^2}{R^2} \frac{\partial^2}{\partial \zeta^2},$$

and $\zeta \equiv \cos \theta$. This is the Grad-Shafranov equation for Ψ (see, e.g., Lovelace et al. 1986). Note that the lines $\Psi(R, \theta) = \text{constant}$ are the poloidal magnetic field lines. Alternatively, the rotation of such a line around the z -axis forms a flux surface.

The magnetic moment of the star is

$$\boldsymbol{\mu} = \frac{1}{2c} \int_{R \leq R_*} d^3x \mathbf{r} \times \mathbf{J} = \mu \hat{\mathbf{z}},$$

where

$$\mu = \frac{\pi}{c} \int_0^{R_*} R^3 dR \int_0^\pi d\theta \sin^2 \theta J_\phi. \quad (4)$$

Initially, before there has been appreciable accretion, we assume that the magnetic moment $\mu_i = \mu(t=0)$ is due to current flow deep inside the star. Thus, the star's initial magnetic field is given by $\Psi_i(R, \theta) = \mu_i \sin^2 \theta / R$ for $R \geq R_*$. Note that $\Delta^* \Psi_i = 0$.

In the following we show that accretion of current-carrying matter to the surface of the star acts to reduce the star's magnetic moment. We consider first the case of a nonconducting star in § 3. In § 4 we consider the realistic case of a highly conducting star.

3. ACCRETION ONTO A NONCONDUCTING STAR

This subsection treats the case of a nonconducting star in order to explain our model of the magnetosphere. This model star has a

nonvarying dipole field source at its center. The magnetic field associated with the accreting matter is allowed to penetrate the star's surface $R = R_*$.

The accreting plasma outside the star is highly conducting. Consequently, plasma falling onto the star carries with it an embedded magnetic field and the associated current density as sketched in Figures 2 and 3. This plasma infall causes the star's magnetic moment to change at the rate

$$\frac{d\mu}{dt} = \frac{\pi}{c} R_*^3 \int_0^\pi d\theta \sin^2 \theta (J_\phi v_R)_{R_*+0}. \quad (5)$$

Here $R_* + 0$ indicates a distance just outside of the star, and v_R is the plasma infall speed, which is approximately the free-fall speed $v_{R_*} = (2GM/R_*)^{1/2}$, because the star's radius R_* is considered to be significantly smaller than the Alfvén radius r_A . This speed is much larger than the rotational velocity of the star's surface $\sim \omega R_*$, because the corotation radius is also considered to be significantly larger than R_* . We assume that there is a strong shock just outside the star's surface that thermalizes the bulk kinetic energy of the flow.

The total magnetic field $\Psi = \Psi_s + \Psi_m$ is the sum of the field due to the star, Ψ_s , and that due to current flow in the magnetosphere, Ψ_m . For the considered conditions where $R_* \ll r_A$, we show below that $|\Psi_m| \ll \Psi_s$. We have $\Psi_s = \mu \sin^2 \theta / R$ far from the star, which satisfies $\Delta^* \Psi_s = 0$. Consequently, equation (3) gives $\Delta^* \Psi_m = -H(\Psi_s) dH(\Psi_s) / d\Psi_s$. Because Ψ_m is small, Ψ (without the s subscript) in subsequent analysis refers to the field of the star.

The funnel flow as shown in Figure 2 exists close to the flux surface $\Psi = \Psi_{\text{ff}} = \mu / r_A$. For a dipole field the funnel flow hits the star's surface at $\theta_{\text{ff}} \approx (R_*/r_A)^{1/2}$. The width in Ψ of the funnel flow is $\Delta \Psi_{\text{ff}} / \Psi_{\text{ff}} \approx \Delta r_A / r_A \ll 1$. The radial width is assumed to be of the order of the half-thickness of the disk h_A at the Alfvén radius r_A as indicated by MHD simulations of funnel flows by Romanova et al. (2002). It is clear that $H(\Psi)$ is zero outside of the funnel flow and that H^2 is a maximum H_m^2 in the middle of the funnel flow at $\Psi = \Psi_{\text{ff}}$. The value of H_m^2 is estimated by the condition that $B_\phi^2 \approx B_p^2$ at the Alfvén radius r_A . For larger values of $(B_\phi/B_p)^2$ at r_A , the magnetic field loop would

open (Lynden-Bell & Boily 1994; Lovelace et al. 1995). Thus, $H_m^2 \approx \mu^2/r_A^4$. This value can be used to show that $|\Psi_m|/\Psi_s \approx (R_*/r_A)^4 \ll 1$.

In equation (5) we can use the fact that

$$J_\phi = \frac{c}{4\pi R \sin \theta} \frac{d}{d\Psi} \frac{H^2}{2}. \quad (6)$$

Thus,

$$\frac{d\mu}{dt} = \frac{1}{4} R_*^2 v_{R*} \int_0^{\pi/2} d\theta \sin \theta \frac{dH^2}{d\Psi} \Big|_{R_*+0}, \quad (7)$$

where we have combined the contributions of the two hemispheres. On the star's surface we have $\Psi = \mu \sin^2 \theta / R_*$ so that $\cos \theta = (1 - R_* \Psi / \mu)^{1/2}$. Thus, we obtain

$$\frac{d\mu}{dt} = \frac{R_*^3 v_{R*}}{8\mu} \int_0^{\mu/R_*} \frac{d\Psi}{(1 - R_* \Psi / \mu)^{1/2}} \frac{dH^2}{d\Psi}. \quad (8)$$

The square root can be Taylor expanded in that $R_* \Psi / \mu \approx R_*/r_A$. An integration by parts then gives

$$\frac{d\mu}{dt} = -\frac{R_*^4 v_{R*}}{16\mu^2} \int_0^{\mu/R_*} d\Psi H^2. \quad (9)$$

Thus, the star's magnetic moment decreases independent of the sign of H and hence independent of the sign of $\omega_K(r_A) - \omega_*$.

Using the mentioned estimates $H_m^2 \approx \mu^2/r_A^4$ and $\Delta\Psi_{\text{ff}} \approx (h_A/r_A)\Psi_{\text{ff}} = (h_A/r_A)(\mu/r_A)$, equation (9) gives

$$\frac{d\mu}{dt} = -\frac{1}{16} \mu \left(\frac{R_*}{r_A}\right)^4 \left(\frac{h_A}{r_A}\right) \left(\frac{v_{R*}}{r_A}\right). \quad (10)$$

This equation is not realistic for a neutron star that is highly conducting.

4. ACCRETION ONTO CONDUCTING STAR

We now treat the case of a highly conducting star. For $R \leq R_*$ the star is considered to be perfectly conducting with the frozen-in dipole magnetic field $\Psi_i = \mu_i \sin^2 \theta / R$. The magnetic field associated with the accreting matter *cannot* penetrate the surface $R = R_*$. The shell from $R = R_*$ to $R_a > R_*$ is the layer of accreted matter. The layer thickness is $R_a - R_* = \Delta R_a \ll R_*$. The accumulated azimuthal current carried by the accretion layer is modeled by surface current layer $\mathcal{K}_\phi(\theta)$ at $R_K = R_* + \Delta R_a/2$.

The magnetic field in the different radial regions can be expanded in terms of solutions of $\Delta^* \Psi = 0$, because the contribution of the magnetospheric currents is negligible. For the region $R > R_K$ we have

$$\Psi^+ = \Psi_i(R, \zeta) + \sum_{n=1,3,\dots} a_n \frac{G_n(\zeta)}{R^n}, \quad (11)$$

where $G_n(\zeta)$ is a Gegenbauer polynomial, $\zeta \equiv \cos \theta$, and the a_n are coefficients determined below. The terms with even values of n are excluded because they correspond to a field that is not mirror symmetric about the $z = 0$ plane. We can take

$$G_n(\zeta) = (1 - \zeta^2) \frac{dP_n(\zeta)}{d\zeta}, \quad (12)$$

where $P_n(\zeta)$ is the usual Legendre polynomial. The other solutions related to the Legendre Q_n functions are unphysical. One can readily show that the G_n obey the orthogonality relations

$$\int_{-1}^1 d\zeta \frac{G_n(\zeta)G_m(\zeta)}{1 - \zeta^2} = \frac{2n(n+1)}{2n+1} \delta_{nm}. \quad (13)$$

For example,

$$G_1 = 1 - \zeta^2, \\ G_3 = -\frac{3}{2} + 9\zeta^2 - \frac{15}{2}\zeta^4,$$

and

$$G_5 = \frac{15}{8} - \frac{225}{8}\zeta^2 + \frac{525}{8}\zeta^4 - \frac{315}{8}\zeta^6.$$

As $\zeta^2 \rightarrow 1$, $G_n \rightarrow n(n+1)(1 - \zeta^2)/2$. As $\zeta \rightarrow 0$ (the equatorial plane), $G_n \rightarrow \sin(\pi n/2)n(n-2)!!/(n-1)!!$, with values of 1, $-3/2$, and $15/8$ for $n = 1, 3$, and 5 .

For $R_* \leq R < R_K$, we have

$$\Psi^- = \Psi_i(R, \zeta) + \sum_{n=1,3,\dots} b_n \left(\frac{1}{R^n} - \frac{R^{n+1}}{R_*^{2n+1}}\right) G_n(\zeta), \quad (14)$$

so that $\Psi(R_*, \zeta) = \Psi_i(R, \zeta)$. For $R \leq R_*$, $\Psi = \Psi_i(R, \zeta)$.

Matching the inner and outer flux functions at $R = R_K$ gives

$$a_n = b_n \left[1 - \left(\frac{R_K}{R_*}\right)^{2n+1} \right]. \quad (15)$$

Evaluation of the jump across the $R = R_K$ surface gives

$$\left(\frac{\partial\Psi^+}{\partial R} - \frac{\partial\Psi^-}{\partial R}\right)_{R_K} = -\sum_{n=1,3,\dots} a_n \frac{G_n(\zeta)}{R_K^{n+1}} \frac{2n+1}{1 - \beta^{2n+1}} \\ = -\frac{4\pi R_K \sin \theta}{c} \mathcal{K}_\phi(\zeta), \quad (16)$$

where $\beta \equiv R_*/R_K < 1$ and $\mathcal{K}_\phi(\zeta)$ is the mentioned surface current density. Thus, we obtain

$$a_n = \frac{4\pi R_K^{n+2}}{c} \frac{1 - \beta^{2n+1}}{2n(n+1)} \int_{-1}^1 d\zeta \frac{\mathcal{K}_\phi(\zeta)G_n(\zeta)}{(1 - \zeta^2)^{1/2}}. \quad (17)$$

Note that a_1 is the contribution to the star's dipole moment due to the surface current \mathcal{K}_ϕ , and a_3 is related to the quadrupole moment because of \mathcal{K}_ϕ . Note also that $1 - \beta^{2n+1} \approx (2n+1)(\Delta R_a/R_*)/2$, which is justified subsequently.

From the considerations of § 3, we have

$$\frac{d\mathcal{K}_\phi}{dt} = (J_\phi v_R)_{R_a}, \quad (18)$$

where J_ϕ is given by equation (6). Thus, we find

$$\frac{da_n}{dt} = \frac{R_*^{n+1} v_{R*}}{4n(n+1)} (1 - \beta^{2n+1}) \int_{-1}^1 d\zeta \frac{dP_n}{d\zeta} \frac{dH^2}{d\Psi} \Big|_{R_a}. \quad (19)$$

In particular,

$$\frac{da_1}{dt} = \frac{1}{4} R_*^2 v_{R_*} (1 - \beta^3) \int_0^{\pi/2} d\theta \sin \theta \left. \frac{dH^2}{d\Psi} \right|_{R_a}, \quad (20)$$

which differs from equation (7) by the factor $1 - \beta^3$. Note that we have neglected the gradual variation of the thickness ΔR_a of the accretion layer. This is justified in § 5.

It is useful in subsequent work to introduce

$$A_1 \equiv \mu_i + a_1, \quad A_n \equiv a_n / R_*^{n-1} \quad (n = 3, 5, \dots), \quad (21)$$

because the A_n all have the same dimensions as the dipole moment.

4.1. Magnetic Energy

The magnetic energy of the system is

$$W = \frac{1}{8\pi} \int d^3x (\mathbf{B}_i + \mathbf{B}')^2 = W_i + W',$$

$$W' = \frac{1}{8\pi} \int d^3x (\mathbf{B}')^2. \quad (22)$$

Here \mathbf{B}_i is the initial dipole field and W_i the associated magnetic energy, which is independent of time. Further, $\mathbf{B}'(t)$ is the field due to the currents on the surface of the star, which result from the accretion, and W' is the associated magnetic energy. The cross term involving $\mathbf{B} \cdot \mathbf{B}'$ in the first line of the equation vanishes because in the volume in which \mathbf{B}' is nonzero ($R \geq R_*$), \mathbf{B}_i can be written as the gradient of a potential. We can also write

$$W' = \frac{1}{2c} \int d^3x J'_\phi A'_\phi.$$

Using equation (16) and equation (13) then gives

$$W' = \frac{1}{R_*^3} \frac{R_*}{\Delta R_a} \sum_{n=1,3,\dots} \frac{n(n+1)}{(2n+1)^2} (A_n - \mu_i \delta_{n0})^2, \quad (23)$$

where δ_{n0} is the Kronecker delta. We have made the approximation $1 - \beta^{2n+1} \approx (2n+1)(\Delta R_a/R_*)/2$, which is justified below, where we estimate ΔR_a .

Most of the magnetic energy W' is in the accretion layer on the star's surface. The reason for this is indicated by the schematic drawing in Figure 3 of the fields \mathbf{B}_i and \mathbf{B}' . The magnetic energy of the \mathbf{B}' field outside of the star ($R \geq R_a$) is

$$W'(\text{ext}) = \frac{1}{4} \int_{-1}^1 d\zeta \int_{R_a}^{\infty} R^2 dR \left[(B'_R)^2 + (B'_\theta)^2 \right]$$

$$= \frac{1}{R_*^3} \sum_{n=1,3,\dots} \frac{n^2(n+1)}{2(2n+1)} (A_n - \mu_i \delta_{n0})^2, \quad (24)$$

where we have replaced R_a with R_* because $\Delta R_a \ll R_*$. Retaining only the $n = 1$ terms gives $W'(\text{ext})/W' = 3\Delta R_a/(2R_*) \ll 1$.

The “buried” magnetic field is predominantly parallel to the star's surface as indicated by Figure 3. The magnetic energy W' of the buried field, denoted B'_\parallel , is approximately equal to $4\pi R_*^2 \Delta R_a (B'_\parallel)^2 / 8\pi$. Retaining only the $n = 1$ term in equation (23) gives the estimate

$$B'_\parallel \sim \frac{2}{3} \frac{R_*}{\Delta R_a} \frac{|A_1 - \mu_i|}{R_*^3}. \quad (25)$$

The buried field strength is enhanced over the initial dipole field (μ_i/R_*^3) by a factor $\approx R_*/\Delta R_a$ for $|A_1| \ll \mu_i$.

4.2. Field at Large Distances from Star

For large R ,

$$\Psi = \frac{A_1 G_1(\zeta)}{R} + \frac{A_3 G_3(\zeta) R_*^2}{R^3} + \dots \quad (26)$$

In the equatorial plane ($\zeta = 0$),

$$\Psi\left(R, \frac{\pi}{2}\right) = \frac{A_1}{R} - \frac{3A_3 R_*^2}{2R^3} + \dots, \quad (27)$$

where $A_1 = \mu_i + a_1$ is the dipole moment at time t . We assume here and subsequently that the decrease in the dipole moment is limited in the respect that

$$A_1 \gg \frac{3|A_3|R_*^2}{2r_A^2}, \quad (28)$$

and $A_1 \gg |A_n G_n(0)|(R_*/r_A)^{n-1}$ for $n = 5, 7, \dots$

Of course, the Alfvén radius r_A depends on the magnetic field in the equatorial plane. This field is

$$B_\theta\left(R, \frac{\pi}{2}\right) = -\frac{A_1}{R^3} + \frac{9A_3 R_*^2}{2R^5} + \dots \quad (29)$$

Owing to inequality (28), $|B_\theta(r_A, \zeta = 0)| = |A_1|/r_A^3$ to a good approximation. For simplicity, we consider that r_A depends only on μ or A_1 and that the other quantities in equation (2) such as M are constant. We then have

$$r_A = r_{Ai} \left(\frac{A_1}{\mu_i} \right)^{4/7}, \quad (30)$$

where r_{Ai} is the Alfvén radius at time $t = 0$. Inequality (28) can then be rewritten as

$$\frac{A_1}{\mu_i} \gg \left| \frac{A_3}{\mu_i} \right|^{7/15} \left(\frac{R_*}{r_{Ai}} \right)^{14/15}. \quad (31)$$

Owing to this inequality,

$$\Psi_{\text{ff}} = \frac{\mu_i}{r_{Ai}} \left(\frac{A_1}{\mu_i} \right)^{3/7}. \quad (32)$$

We assume that $h_A/r_A = \text{constant} \ll 1$, so that $\Delta\Psi_{\text{ff}}/\Psi_{\text{ff}} = h_{Ai}/r_{Ai} = \text{constant} \ll 1$. From § 3 we have $H_m = A_1^2/r_A^4$. Thus,

$$H_m^2 = \frac{\mu_i^2}{r_{Ai}^4} \left(\frac{\mu_i}{A_1} \right)^{2/7}. \quad (33)$$

4.3. Dimensionless Variables

It is natural to measure the magnetic moment A_1 in units of its initial value μ_i ,

$$\tilde{A}_1 \equiv \frac{A_1}{\mu_i}, \quad \tilde{A}_n \equiv \frac{A_n}{\mu_i} \quad (n = 3, 5, \dots), \quad (34)$$

with the tildes indicating the dimensionless variables. We measure Ψ in units of μ_i/R_* and $B_R(R_*, \zeta)$ in units of μ_i/R_*^3 . In terms

of the dimensionless variables, $\tilde{B}_R(R_*, \zeta) = -d\tilde{\Psi}/d\zeta$. Further we have

$$\tilde{\Psi}_{\text{ff}} = \frac{R_*}{r_{\text{Ai}}} \tilde{A}_1^{3/7}, \quad \text{and} \quad \Delta\tilde{\Psi}_{\text{ff}} = \frac{R_* h_{\text{Ai}}}{r_{\text{Ai}} r_{\text{Ai}}} \tilde{A}_1^{3/7}, \quad (35)$$

from equation (35).

In subsequent work we drop the tildes from the A_n and Ψ .

4.4. Specific Model for $H(\Psi)$

The qualitative dependence of $H(\Psi)$ is discussed in § 3. A specific function with this dependence is

$$[H(\Psi)]^2 = H_m^2 \exp\left[-\frac{(\Psi - \Psi_{\text{ff}})^2}{2\Delta\Psi_{\text{ff}}^2}\right]. \quad (36)$$

We can now rewrite equation (19) in dimensionless form as

$$\frac{dA_n}{d\tau} = -\frac{2n+1}{n(n+1)} \frac{\mathcal{I}_n}{A_1^{5/7}}. \quad (37)$$

Here

$$\mathcal{I}_n \equiv \int_0^1 d\zeta \frac{dP_n}{d\zeta} X \exp\left(-\frac{X^2}{2}\right), \quad X(\zeta) \equiv \frac{\Psi(\zeta) - \Psi_{\text{ff}}}{\Delta\Psi_{\text{ff}}},$$

where $\Psi(\zeta) \equiv \Psi(R_*, \zeta)$, with

$$\Psi(\zeta) = \sum_{n=1,3,\dots} A_n G_n(\zeta).$$

The dimensionless time variable τ is given by

$$\frac{dt}{d\tau} = 4 \left(\frac{r_{\text{Ai}}}{R_*}\right)^3 \frac{R_*}{v_{R_*}} \frac{\Delta\Psi_{\text{ff}}}{\Psi_{\text{ff}}} \frac{R_*}{\Delta R_a(t)}. \quad (38)$$

The initial conditions for equation (37) are $A_1(0) = 1$ and $A_n(0) = 0$ for $n = 3, 5, \dots$

For simplicity, we consider $\Delta\Psi_{\text{ff}}/\Psi_{\text{ff}}$ to be a fixed number small compared with unity. Consequently, the solution of equation (37) depends on the dimensionless time τ and on two dimensionless parameters, \mathcal{E} and ϵ ,

$$A_n = A_n(\tau, \mathcal{E}, \epsilon), \quad \mathcal{E} \equiv \frac{R_*}{r_{\text{Ai}}}, \quad \epsilon \equiv \frac{\Delta\Psi_{\text{ff}}}{\Psi_{\text{ff}}} = \frac{h_{\text{Ai}}}{r_{\text{Ai}}}, \quad (39)$$

where $\mathcal{E} \ll 1$ and $\epsilon \ll 1$.

4.5. Single Mode, $A_1 \neq 1$

For the special case of *only* one mode $A_1 \neq 0$, equation (37) can be approximated analytically. We find

$$\mathcal{I}_1 = -\frac{A_1^{4/7}}{\epsilon\mathcal{E}} \int_0^1 d\zeta (\zeta^2 - Z) \exp[-k(\zeta^2 - Z)^2]. \quad (40)$$

Here $k \equiv A_1^{8/7}/(2\epsilon^2\mathcal{E}^2)$ and $Z \equiv 1 - \mathcal{E}/A_1^{4/7}$, where we assume that $Z > 0$ or $A_1 > \mathcal{E}^{7/4}$. Because $\epsilon \ll 1$, $k \gg 1$, so that equation (40) can be evaluated easily as

$$\mathcal{I}_1 \approx -\frac{\sqrt{\pi/2}}{2} \frac{\epsilon^2\mathcal{E}^2}{A_1^{8/7}Z^{3/2}}. \quad (41)$$

Thus, we find

$$\begin{aligned} \frac{dA_1}{d\tilde{\tau}} &= -1 \text{ or } A_1 = 1 - \tilde{\tau} \quad (0 \geq \tilde{\tau} \leq 1), \\ \frac{dt}{d\tilde{\tau}} &= \frac{16\sqrt{2}}{3\sqrt{\pi}} \frac{A_1^{13/7}}{\epsilon\mathcal{E}^5} \frac{R_*}{v_{R_*}} \frac{R_*}{\Delta R_a}. \end{aligned} \quad (42)$$

We have used the approximation $Z = 1$, which assumes that $A_1 \gg \mathcal{E}^{7/4} \ll 1$.

Equation (42) can be solved to give

$$t = t_0 \left[1 - (1 - \tilde{\tau})^{20/7}\right].$$

Here

$$t_0 = \frac{28\sqrt{2}}{15\sqrt{\pi}} \frac{R_*}{v_{R_*}} \frac{1}{\epsilon\mathcal{E}^5} \frac{R_*}{\langle\Delta R_a\rangle} \quad (43)$$

is the timescale for the field decrease. This equation can also be written as

$$t_0 \approx 1.5 \frac{R_*}{v_{R_*}} \frac{r_{\text{Ai}}}{h_{\text{Ai}}} \left(\frac{r_{\text{Ai}}}{R_*}\right)^5 \frac{R_*}{\langle\Delta R_a\rangle}.$$

Here $\langle\Delta R_a\rangle$ is the time-averaged thickness of the accretion layer, where it is assumed that ΔR_a varies gradually with time. For a neutron star of mass $M = 1.4 M_\odot$ and radius $R_* = 10^6$ cm, we find

$$t_0 \approx 0.78 \times 10^5 \left(\frac{0.001}{\epsilon}\right) \left(\frac{0.005}{\mathcal{E}}\right)^5 \left(\frac{100}{R_*/\langle\Delta R_a\rangle}\right) \text{ yr}. \quad (44)$$

The normalization of \mathcal{E} or, equivalently, r_{Ai} , follows from equation (2). The normalization of ϵ or, equivalently, $h_{\text{Ai}}/r_{\text{Ai}}$, is based on the Shakura-Sunyaev (1973) disk model, which indicates that ϵ depends quite weakly on the different parameters (e.g., $\epsilon \propto \dot{M}^{1/5}$). The normalization of $R_*/\langle\Delta R_a\rangle$ is discussed in § 5. The shortness of this timescale is due to the fact that only one mode is accounted for.

4.6. Numerical Integrations

The results of § 4.5 for a single mode point out the importance of using a new time variable in place of τ in equation (37). That is, we rewrite this equation as

$$\frac{dA_n}{d\tau'} = -\frac{2n+1}{n(n+1)} A_1^{8/7}(\tau') \mathcal{I}_n(\tau'), \quad (45)$$

for $n = 1, 3, \dots$, where

$$\frac{d\tau}{d\tau'} = A_1^{13/7}(\tau'). \quad (46)$$

Combining this equation with equation (38) gives

$$\frac{dt}{d\tau'} = 4 \frac{\epsilon}{\mathcal{E}^3} \frac{R_*}{v_{R_*}} \frac{R_*}{\langle\Delta R_a\rangle} A_1^{13/7}. \quad (47)$$

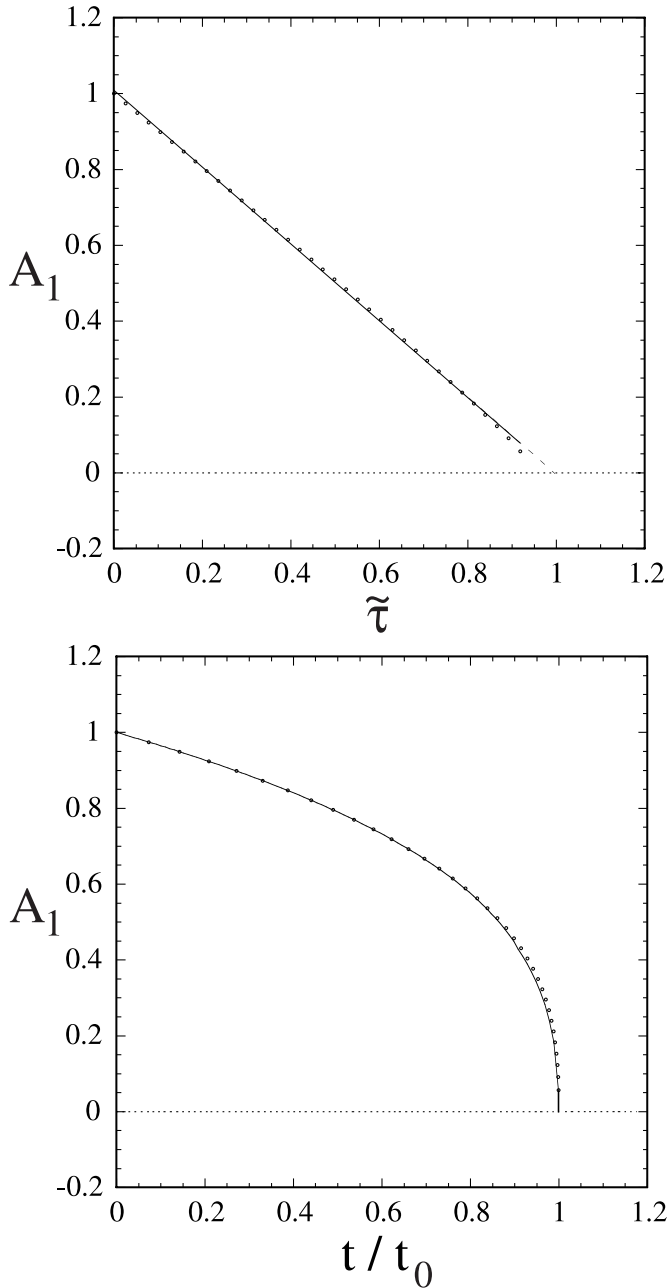


FIG. 4.—Time dependence of the normalized magnetic moment A_1/μ_i for the special case of only the dipole mode. Here μ_i is the initial magnetic moment of the star, and t_0 is given by eq. (43).

We let τ_0 and τ'_0 denote the values for which $A_1 \leq 0.01$. We have

$$\tau_0 = \int_0^{\tau'_0} d\tau' A_1^{13/7}(\tau'). \quad (48)$$

The corresponding actual time when $A_1 \leq 0.01$ is

$$t_0 = 4 \frac{\epsilon R_*}{\mathcal{E}^3 v_{R*}} \frac{R_*}{\langle \Delta R_a \rangle} \tau_0(\mathcal{E}, \epsilon). \quad (49)$$

For the case of a single mode (A_1), τ' is proportional to $\tilde{\tau}$ (neglecting the weak time dependence of ΔR_a). For this case A_1 decreases linearly with $\tilde{\tau}$ or τ' .

We find equation (45) to be stiff. For this reason a predictor-corrector code (Gear 1971, chap. 9) was developed and used to

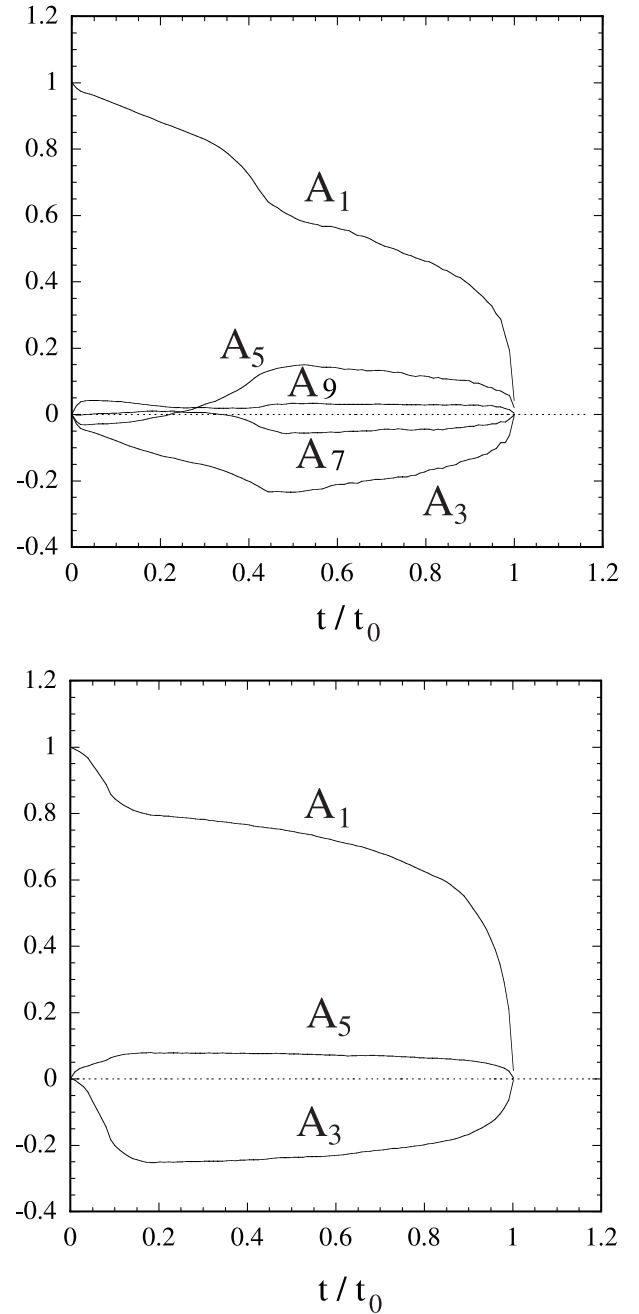


FIG. 5.—Time dependence of the normalized magnetic multipole moments. The top panel is for a case with five modes for $\mathcal{E} = 0.05$ and $\epsilon = 0.1$, while the bottom panel is for three modes for $\mathcal{E} = 0.025$ and $\epsilon = 0.05$. The time t_0 is given by equation (51).

solve the equations for one, three, and five modes. The integrals \mathcal{I}_n were evaluated using a stretched ζ grid with 10^4 – 10^5 intervals. Figure 4 shows the numerical solution for the case of one mode (A_1). This agrees closely with the analytic solution of § 4.5.

Figure 5 shows sample results for cases of three and five modes. The timescales $t_0(\mathcal{E}, \epsilon)$ for three and five modes are not appreciably different. Combining the results of many runs for $\mathcal{E} = 0.01$ – 0.1 and $\epsilon = 0.02$ – 0.1 we find

$$\tau_0 \approx \frac{1.2 \times 10^{-4}}{\mathcal{E}^{3.6} \epsilon^{2.7}}. \quad (50)$$

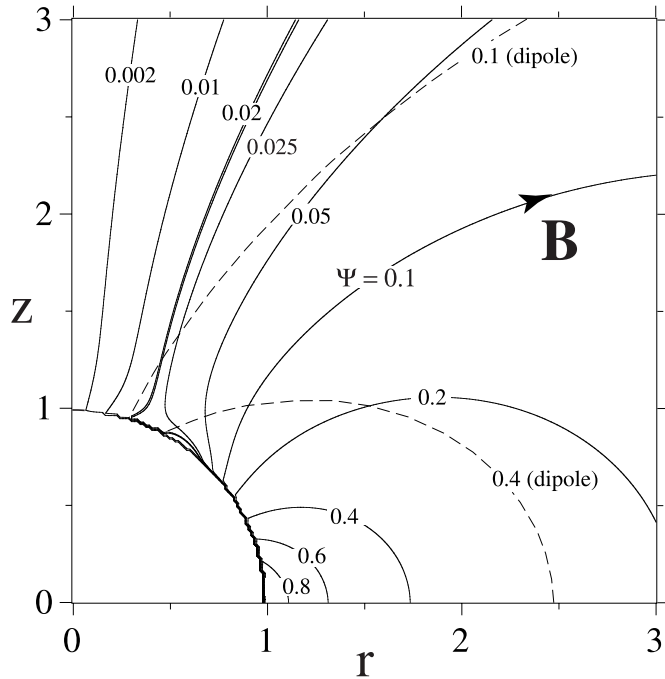


FIG. 6.—Magnetic field lines of a screened star (solid lines) with three modes at $t/t_0 = 0.85$ when $A_1 \approx 0.59$, $A_3 \approx -0.19$, and $A_5 \approx 0.062$ for a case with $\mathcal{E} = 0.025$ and $\epsilon = 0.025$. The dashed lines are for the initial, pure dipole field. The thicker line $\Psi = \mathcal{E}A_1^{3/7} \approx 0.02$ is the centroid of the funnel flow. It is clear from this figure that the star's field is markedly changed by the accretion.

The integrations become increasingly long as ϵ and \mathcal{E} decrease. In view of equation (49) we have

$$t_0 \approx 1.6 \times 10^7 \left(\frac{0.001}{\epsilon} \right)^{1.7} \left(\frac{0.005}{\mathcal{E}} \right)^{6.6} \left(\frac{100}{R_*/\langle \Delta R_a \rangle} \right) \text{ yr.} \quad (51)$$

This timescale is considerably longer than that for the case of the single mode (eq. [44]). The timescale varies approximately as $\mu_i^{3.8}/M^{1.9}$. Thus, for a neutron star with an initial surface magnetic field of 2×10^{12} G or $\mu_i = 2 \times 10^{30}$ G cm³, the timescale of equation (51) increases to 2.2×10^8 yr.

Figure 6 shows the magnetic field lines at a time during the evolution and the initial, pure dipole field. Figure 7 shows the corresponding surface current density on the star's surface.

5. ACCRETION LAYER THICKNESS

We now give a rough estimate of the accretion layer thickness ΔR_a . We let ΔM denote the mass accreted after time t , which is in a layer of thickness $\Delta R_a \ll R_*$. The mean density of the layer is thus $\bar{\rho} \sim \Delta M/(4\pi R_*^2 \Delta R_a)$. The change in pressure across the layer in hydrostatic equilibrium is $p \sim [\Delta M/(4\pi R_*^2)]g$, where $g = GM/R_*^2 \approx 1.87 \times 10^{14}$ cm s⁻². The equation of state of the neutron star matter gives $p \approx k(\bar{\rho})^n$ with $k \approx 2.1 \times 10^{11}$ in cgs units, and $n \approx 1.5$ (Baym et al. 1971). Thus, we obtain

$$\begin{aligned} \Delta R_a &\sim \left(\frac{k}{g} \right)^{1/n} \left(\frac{\Delta M}{4\pi R_*^2} \right)^{(n-1)/n} \\ &\sim 1.3 \times 10^4 \left(\frac{\Delta M}{10^{-2} M_\odot} \right)^{1/3} \text{ cm.} \end{aligned} \quad (52)$$

For $\Delta R_a = 10^4$ cm, equation (25) gives an estimate of the buried magnetic field of $\sim 6.7 \times 10^{13}$ G. Thus, the magnetic pressure in the accretion layer is negligible compared to the matter pressure.

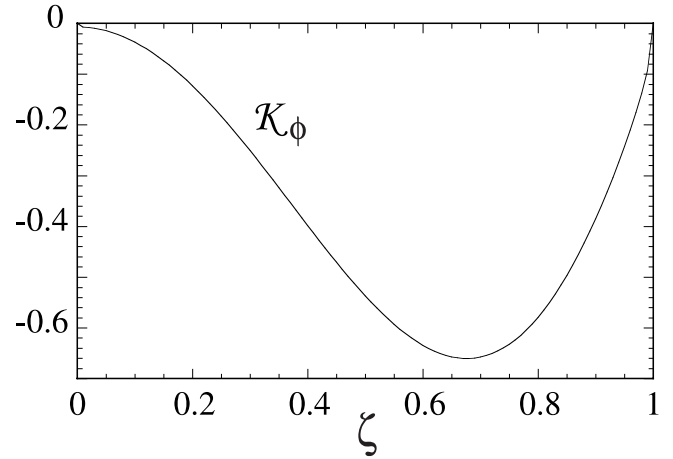


FIG. 7.—Surface current density \mathcal{K}_ϕ is shown as a function of $\zeta = \cos(\theta)$, with θ the colatitude, for the same case as Figure 6. The vertical scale is arbitrary.

5.1. Ohmic Diffusion of the Field

The influence of Ohmic diffusion on the “burial” of magnetic field during accretion to a neutron star has been studied by Cumming et al. (2001). They treat the competition between the inward advection of the magnetic field inside the star and the tendency of the field to diffuse outward as a result of the finite conductivity of the plasma. For sufficiently large accretion rates (such as that considered here) the inward advection is found to be larger than the diffusion.

Magnetic field buried during intensive accretion will Ohmically diffuse out of the star after the accretion stops (BK74). The timescale for the buried field to diffuse out of the star can be estimated as

$$t_{\text{Ohm}} \sim \frac{(\Delta R_a)^2}{\eta}, \quad \eta = \frac{c^2}{4\pi\sigma}, \quad (53)$$

where η is the magnetic diffusivity and σ is the conductivity. Using the Cumming et al. (2001; see their § 2.2) formula for the conductivity and our normalization values we find

$$t_{\text{Ohm}} \sim 2.7 \times 10^9 \left(\frac{\Delta R_a}{10^4 \text{ cm}} \right) \left(\frac{\Delta M}{10^{-2} M_\odot} \right) \text{ yr.} \quad (54)$$

Thus, it takes a rather long time for the field to diffuse out of the star.

It is possible that the buried magnetic field is subject to the interchange or buoyancy instabilities considered by Cumming et al. (2001) and by Kato et al. (1998, chap. 17), but the detailed analysis is beyond the scope of the present work.

6. CONCLUSIONS

An analytical model is developed for the screening of the external magnetic field of a rotating, magnetized, axisymmetric neutron star due to the accretion of plasma from a disk. The decrease of the field occurs as a result of the deposition of current-carrying plasma onto the star's surface. This plasma creates an induced magnetic moment with a sign opposite to that of the original magnetic dipole. The physical mechanism is explained in Figure 3. Equation (37) for the field evolution is inherently nonlinear, and this leads to the generation of higher order modes when starting from the lowest order mode.

The main conclusions from this work are: (1) the field decreases independent of whether the star spins up or spins down (that is, for $r_{\text{cr}} > r_A$ or $r_{\text{cr}} < r_A$); (2) the timescale for an appreciable decrease (by a factor >100) of the field is $t_0 \sim 1.6 \times 10^7$ yr for $\dot{M} = 10^{-9} M_{\odot} \text{ yr}^{-1}$ and an initial stellar magnetic moment $\mu_i = 10^{30} \text{ G cm}^3$, and it scales approximately as $\mu_i^{3.8} / \dot{M}^{1.9}$; (3) the decrease of the magnetic field does not have a simple relation to the accreted mass; (4) at late times the magnitude of the buried magnetic field is much larger than the initial field on the star's surface; and (5) once the accretion stops the field leaks out on an Ohmic diffusion timescale, which is estimated to be $\gtrsim 10^9$ yr.

The present model has evident limitations that require further study: accreting neutron stars are not expected to have their magnetic and rotational axes aligned. The case of small misalignment angles may be amenable to analytic treatment. The thickness of the accretion layer will in general be a function of position.

We thank Dong Lai for a number of valuable discussions. We also thank the referee for valuable recommendations. This work was supported in part by NASA grant NAG5-13220 and NSF grant AST 03-07817.

REFERENCES

- Baym, G. H., Bethe, H. A., & Pethick, C. J. 1971, *Nucl. Phys. A*, 175, 225
 Bhattacharya, D., & van den Heuvel, E. P. J. 1991, *Phys. Rep.*, 203, 1
 Bisnovatyi-Kogan, G. S., & Komberg, B. V. 1974, *AZh*, 51, 373 (English transl. in *Soviet Astron.*, 18, 217 [1975])
 Cheng, K. S., & Zhang, C. M. 1998, *A&A*, 337, 441
 ———. 2000, *A&A*, 361, 1001
 Choudhuri, A. R., & Konar, S. 2002, *MNRAS*, 332, 933
 Cumming, A., Zweibel, E., & Bildsten, L. 2001, *ApJ*, 557, 958
 Gear, C. W. 1971, *Numerical Initial Value Problems in Ordinary Differential Equations* (Englewood Cliffs: Prentice-Hall)
 Ghosh, P., & Lamb, F. K. 1979, *ApJ*, 232, 259
 Gold, T., & Hoyle, F. 1960, *MNRAS*, 120, 89
 Goldreich, P., & Reisenegger, A. 1992, *ApJ*, 395, 250
 Hulse, R. A., & Taylor, J. H. 1975, *ApJ*, 195, L51
 Illarionov, A. F., & Sunyaev, R. A. 1975, *A&A*, 39, 185
 Kato, S., Fukue, J., & Mineshige, S., ed. 1998, *Black-Hole Accretion Disks* (Kyoto: Kyoto Univ. Press)
 Long, M., Romanova, M. M., & Lovelace, R. V. E. 2004, *ApJ*, submitted
 Lorimer, D. R. 2001, *Living Reviews in Relativity*, 4, 5
 Lovelace, R. V. E., Mehanian, C., Mobarry, C. M., & Sulkanen, M. E. 1986, *ApJS*, 62, 1
 Lovelace, R. V. E., Romanova, M. M., & Bisnovatyi-Kogan, G. S. 1995, *MNRAS*, 275, 244
 ———. 1999, *ApJ*, 514, 368
 Lynden-Bell, D., & Boily, C. 1994, *MNRAS*, 267, 146
 Lyne, A. G., et al. 2004, *Science*, 303, 1153
 Payne, D. J. B., & Melatos, A. 2004, *MNRAS*, 351, 569
 Romani, R. W. 1990, *Nature*, 347, 741
 Romanova, M. M., Ustyugova, G. V., Koldoba, A. V., & Lovelace, R. V. E. 2002, *ApJ*, 578, 420
 ———. 2004, *ApJ*, 616, L151
 Ruderman, M. 1991, *ApJ*, 366, 261
 Shakura, N. I., & Sunyaev, R. A. 1973, *A&A*, 24, 337
 Trimble, V., & Rees, M. 1970, in *IAU Symp. 46, The Crab Nebula*, ed. R. D. Davies & F. Graham-Smith (Dordrecht: Reidel), 273
 van den Heuvel, E. P. J., & Bitzaraki, O. 1995, *A&A*, 297, L41
 Wijers, R. A. M. J. 1997, *MNRAS*, 287, 607